
AORTADIFF: A UNIFIED MULTITASK DIFFUSION FRAMEWORK FOR CONTRAST-FREE AAA IMAGING

Yuxuan Ou¹, Ning Bi², Jiazheng Pan³, Jiancheng Yang⁴⁵, Boliang Yu², Usama Zidan², Regent Lee², Vicente Grau¹

¹Department of Engineering Science, University of Oxford, United Kingdom

²Nuffield Department of Surgical Sciences, University of Oxford, United Kingdom

³Technical University of Munich, Germany

⁴ELLIS Institute Finland, Finland

⁵Aalto University, Finland

yuxuan.ou@trinity.ox.ac.uk, ning.bi@nds.ox.ac.uk,
 jiazheng.pan@tum.de, jiancheng.yang@aalto.fi, boliang.yu@nds.ox.ac.uk,
 usama.zidan@nds.ox.ac.uk, regent.lee@nds.ox.ac.uk, vicente.grau@eng.ox.ac.uk

October 3, 2025

ABSTRACT

While contrast-enhanced CT (CECT) is standard for assessing abdominal aortic aneurysms (AAA), the required iodinated contrast agents pose significant risks, including nephrotoxicity, patient allergies, and environmental harm. To reduce contrast agent use, recent deep learning methods have focused on generating synthetic CECT from non-contrast CT (NCCT) scans. However, most adopt a multi-stage pipeline that first generates images and then performs segmentation, which leads to error accumulation and fails to leverage shared semantic and anatomical structures. To address this, we propose a unified deep learning framework that generates synthetic CECT images from NCCT scans while simultaneously segmenting the aortic lumen and thrombus. Our approach integrates conditional diffusion models (CDM) with multi-task learning, enabling end-to-end joint optimization of image synthesis and anatomical segmentation. Unlike previous multitask diffusion models, our approach requires no initial predictions (e.g., a coarse segmentation mask), shares both encoder and decoder parameters across tasks, and employs a semi-supervised training strategy to learn from scans with missing segmentation labels, a common constraint in real-world clinical data. We evaluated our method on a cohort of 264 patients, where it consistently outperformed state-of-the-art single-task and multi-stage models. For image synthesis, our model achieved a PSNR of 25.61 dB, compared to 23.80 dB from a single-task CDM. For anatomical segmentation, it improved the lumen Dice score to 0.89 from 0.87 and the challenging thrombus Dice score to 0.53 from 0.48 (nnU-Net). These segmentation enhancements led to more accurate clinical measurements, reducing the lumen diameter MAE to 4.19 mm from 5.78 mm and the thrombus area error to 33.85% from 41.45% when compared to nnU-Net. Code is publicly available at <https://github.com/yuxuanou623/AortaDiff.git>.

1 Introduction

Clinical assessment of vascular conditions like abdominal aortic aneurysms (AAA) traditionally relies on contrast-enhanced CT (CECT), where an intravenous iodinated contrast agent illuminates the aortic lumen to reveal abnormalities such as thrombus [1]. However, this procedure poses risks to patients with renal insufficiency or contrast allergies, involves uncomfortable needle insertions, and contributes to environmental iodine waste [2, 3, 4]. This has created a significant clinical need for an advanced method capable of performing AAA assessment solely on non-contrast CT (NCCT) scans. Such an approach is particularly challenging because thrombus and blood are nearly indistinguishable in NCCT, as shown in Figure 1 (b). Recent advances in deep learning offer a promising pathway to overcome this diagnostic challenge. An effective AI solution must therefore perform two interrelated tasks: (1) generate a realistic

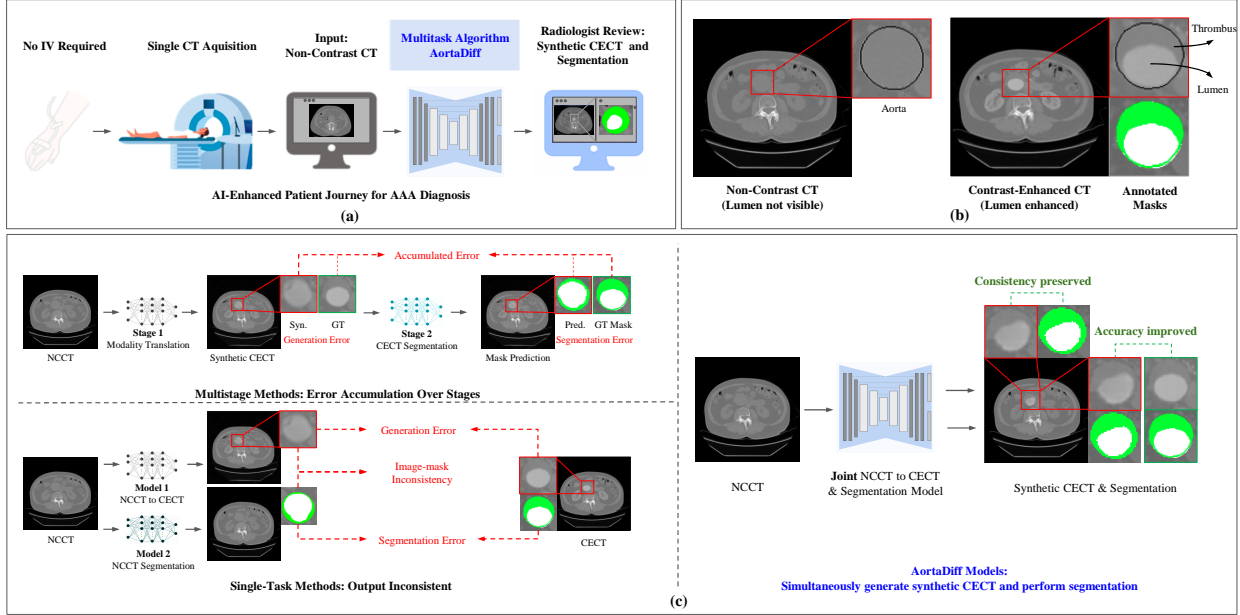


Figure 1: Unified Multitask Framework for Contrast-Free AAA Assessment. This figure illustrates the clinical motivation, CT imaging concepts, and advantages of our proposed multitask diffusion model (AortaDiff) over traditional approaches. **(a)** The proposed AI-enhanced clinical workflow enables diagnosis from a NCCT scan, eliminating the need for intravenous (IV) contrast agents. **(b)** A visual comparison highlights the diagnostic challenge: the aortic lumen is obscured in the NCCT but is clearly delineated in the CECT. **(c)** Our unified multitask model is contrasted with prior methods. Multistage pipelines risk accumulating synthesis errors into the final segmentation. Single-task approaches can produce segmentations that are inconsistent with the synthesized image. In contrast, our end-to-end model jointly generates a high-fidelity synthetic CECT and an accurate, consistent segmentation mask.

synthetic CECT to aid visual interpretation by radiologists, and (2) accurately segment the aortic lumen, allowing thrombus to be identified as the non-enhancing regions outside this segmented area. This dual-output approach provides radiologists with both a qualitative view of the anatomy from the synthetic image and immediate quantitative measurements of the abnormality from the segmentation mask, as illustrated in Figure 1 (a).

Recent AI advancements have primarily focused on generating synthetic CECTs from NCCT scans, exploring architectures from early CNNs [5] to GANs [6, 7, 8] and Transformers [9]. However, these works are constrained by a fundamental limitation: they frame the problem as a single-task, image-to-image translation. This overlooks the clinical reality that a visually plausible image is not the end goal, but an intermediate step towards quantitative analysis. Consequently, when segmentation is required, it is relegated to a separate, downstream model [7, 8]. This multi-stage pipeline is inherently flawed, as it is susceptible to error accumulation—where synthesis artifacts degrade segmentation accuracy—and inhibits knowledge sharing between the two synergistic tasks.

To address the shortcomings of multi-stage methods, some pioneering works have explored unified, multi-task frameworks. For instance, Hu et al. [10] and UCAS [11] proposed models that jointly perform CECT synthesis and segmentation. However, these early multi-task attempts are predominantly built upon GAN-based architectures. While innovative in their task formulation, they inherit the well-known challenges of GANs: they often produce overly smooth outputs that lack the sharp anatomical boundaries critical for clinical diagnosis and can suffer from training instability or mode collapse [12]. Therefore, a significant gap remains for a framework that not only adopts a unified multi-task design but also leverages a more powerful generative model to ensure both high-fidelity synthesis and precise, simultaneous segmentation.

To address these limitations, we propose a unified multi-task diffusion framework (AortaDiff) that jointly performs image translation from NCCT to CECT and lumen segmentation. The core of our approach is a novel denoising U-Net architecture featuring a shared encoder-decoder backbone that ends in two different prediction heads: one for the denoised image and one for the segmentation mask. This single-backbone design allows the network to learn a rich, shared latent representation that includes both texture of contrast enhancement and precise anatomical information

about lumen thrombus boundary. What’s more, our model advances beyond prior multitask diffusion methods in two ways. First, it operates directly on the raw NCCT input, eliminating the need for any coarse initial predictions (e.g., a pre-computed coarse segmentation mask) during both training and inference. Second, to address the specific challenge of scarce lumen segmentation labels, we introduce a semi-supervised training strategy. This strategy incorporates a loss function that dynamically changes between supervised objectives on fully labeled data with an unsupervised reconstruction objective on image-only pairs. This allows our model to effectively leverage the entire dataset, even when only a subset of scans have lumen masks, enhancing its generalization capabilities under limited supervision and aligning with the practical constraints of clinical data acquisition.

We conducted a comprehensive evaluation of our framework on the Oxford Abdominal Aortic Aneurysm (OxAAA) dataset [13]. Our unified model was benchmarked against state-of-the-art baselines and traditional multi-stage pipelines. The results demonstrate a significant and consistent improvement across all tasks. For the challenging thrombus segmentation, our model increases the Dice score from 0.48 (nnU-Net) to 0.53, and for lumen segmentation, from 0.87 to 0.89. In the synthesis task, our framework achieves a PSNR of 25.61 dB, markedly outperforming the single-task CDM’s 23.80 dB. Qualitatively, our jointly generated outputs exhibit sharper anatomical details and superior segmentation consistency. We also validate our method on two AAA clinical measurements and found that it yields more accurate morphological predictions for both lumen diameter and thrombus area, underscoring its potential for reliable clinical application.

In summary, the contributions of this work are threefold:

- We propose a novel diffusion-based multi-task framework designed to move beyond simple image synthesis towards clinically actionable analysis. Based on the insight that a synthetic CECT is an intermediate step, our model jointly performs synthetic CECT generation and lumen segmentation. This integrated approach enables a safer and more sustainable workflow for AAA imaging by reducing the need for contrast agent injection.
- To address the real-world challenge of missing lumen segmentation annotations, we introduce a semi-supervised strategy that enables effective learning from datasets where only a subset of image pairs contains lumen segmentation masks. This strategy improves both generation and segmentation performance beyond fully supervised training, leveraging cross-task consistency and multi-task representation learning.
- Experiments on the OxAAA dataset demonstrate that our model outperforms all single-task baselines and multi-stage pipelines on both generation and segmentation tasks. Our method is also more label-efficient than prior multi-task diffusion approaches, making it suitable for scalable deployment in resource-constrained healthcare environments.

2 Related Work: Multi-task Diffusion Models

Extending diffusion models for multi-task learning is an active area of research, with many foundational strategies first developed in general computer vision. For instance, CoDi [14] enables ‘any-to-any’ generation by aligning separate, pre-trained diffusers in a shared latent space via cross-attention. TaskDiffusion [15] introduces a joint denoising process with a cross-task decoder to unify dense predictions, while DiffusionMTL [16] uses a shared encoder that branches into task-specific decoders, conditioning the diffusion process on their initial outputs. Other works, like Shadow Diffusion [17], require a coarse initial mask to guide the joint refinement process. Focusing on efficiency, MTU [18] adapts pre-trained models by replacing network layers with smaller, task-specific feed-forward network and proposing a routing mechanism. While these general-purpose frameworks are foundational, they are not tailored for the unique constraints of medical imaging, such as the need for high anatomical precision and handling of scarce clinical data.

Within the medical domain, a few works have begun to adapt these concepts. DiffAtlas [19], for example, applied a joint image-mask generation model to medical images but was limited by its requirement for full supervision. While all these works have significantly advanced multi-task diffusion, a critical gap remains for a framework that is simultaneously (1) architecturally unified and specialized for a spatially coherent medical task, (2) initialization-free and label-efficient via a semi-supervised scheme, and (3) validated on a high-stakes clinical application. Our work is designed to fill this specific void.

3 Proposed Method: AortaDiff

We propose AortaDiff, a novel multi-task diffusion-based framework that jointly generates synthetic CECT images and performs lumen segmentation directly from NCCT scans. The method focuses explicitly on the aortic region, simultaneously synthesizing the CECT image and its corresponding lumen mask while preserving the surrounding

background. Furthermore, we employ a semi-supervised training strategy that effectively learns both tasks by leveraging a combination of data with and without lumen mask annotations.

Example of a Misaligned Image Pair

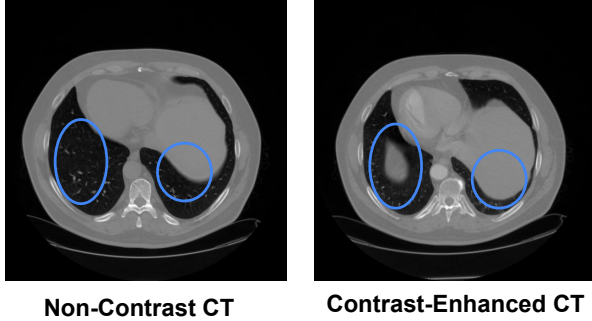


Figure 2: **Misalignments in Paired Scans from the OxAAA Dataset.** An example of spatial discrepancies between corresponding NCCT and CECT slices from the OxAAA dataset. This illustrates the inherent difficulty of achieving perfect pixel-wise alignment in practice, even after standard registration.

3.1 Aorta-focused Generation with Background Preservation

A primary challenge in paired NCCT-CECT datasets is spatial misalignment due to factors like respiratory motion, even after standard image registration [12]. An example is shown in Figure 2. To prevent the model from learning spurious translations of surrounding tissues, such as the airways, we constrain the generative process to focus exclusively on the aortic region, shown in Figure 1 (b), while preserving the original NCCT background.

Aorta-Focused Training Strategy Inspired by [20], our training objective is localized to a bounding box tightly enclosing the aorta, which is determined from the ground truth aorta segmentation masks. Within this bounding box, we replace the standard pixel-wise MSE loss with a perceptual loss \mathcal{L}_p [21]. This loss is less sensitive to the minor pixel shifts inherent in misaligned data and encourages the model to reconstruct the aorta texture and morphology faithfully. The reconstruction loss is therefore calculated as:

$$\mathcal{L}_{\text{recon}} = \mathcal{L}_p(\mathbf{x}_0[\mathbb{B}], \hat{\mathbf{x}}_0[\mathbb{B}]), \quad (1)$$

where \mathbf{x}_0 and $\hat{\mathbf{x}}_0$ are the ground truth and predicted CECT images, respectively, and \mathbb{B} denotes the patch defined by the aorta-enclosing bounding box.

Inference and Fusion Strategy During inference, we first obtain an aorta segmentation mask on NCCT scans using a pre-trained nnU-Net. It is trained exclusively on the training split with strict patient-level separation, using only NCCT scans and aorta labels. The model is frozen before any test evaluation and achieves a Dice score of 0.93 on the validation set. To generate the final image while preserving the background, we adapt the inpainting strategy from RePaint [22]. At each denoising timestep t , the known background region is directly replaced by the corresponding pixels from the input NCCT scan after applying the forward diffusion process noise scheduled for that step. Concurrently, the foreground aorta region is filled with our model’s denoised prediction. This composition ensures a seamless fusion of the synthesized aorta into its original anatomical context. To further enhance boundary coherence, we employ a resampling scheme [22], where the denoising process is interleaved with several noising steps, allowing the model to better harmonize the foreground and background.

3.2 A Unified Architecture for Multitask Denoising

To enable multi-task learning, we adapt the standard denoising U-Net architecture to simultaneously predict both the denoised image and its corresponding lumen segmentation. We implement this by incorporating two parallel prediction heads that branch from the final layer of the shared U-Net decoder. The first head outputs the predicted image noise, as is standard in DDPMs. For the second head, to encourage smoother and more precise lumen boundary prediction, we represent the lumen mask as a Signed Distance Function (SDF). This head therefore outputs a predicted SDF, \hat{s}_0 . This unified design forces the shared backbone to learn a rich latent representation beneficial for both tasks. To balance these

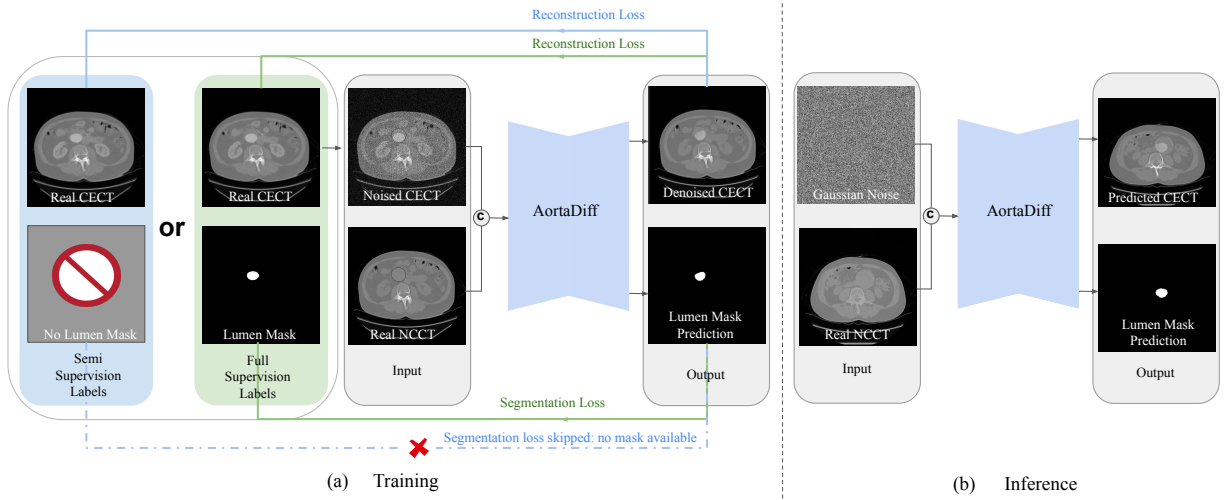


Figure 3: Overview of the AortaDiff Training and Inference Workflow. The model is trained using a semi-supervised strategy. For all data, the model is updated with a reconstruction loss. An additional segmentation loss is applied only when a lumen mask is available. In inference, starting with an NCCT scan and a pure Gaussian noise image, the model performs iterative denoising to jointly generate a synthetic CECT and its corresponding lumen mask.

distinct objectives, we employ the principled uncertainty-weighting strategy from Kendall et al. [23]. This approach introduces two trainable parameters, σ_1 and σ_2 , to automatically learn the task weightings by optimizing the joint objective:

$$\mathcal{L}(W, \sigma_1, \sigma_2) = \frac{1}{2\sigma_1^2} \mathcal{L}_{\text{seg}}(W) + \frac{1}{2\sigma_2^2} \mathcal{L}_{\text{recon}}(W) + \log(\sigma_1\sigma_2), \quad (2)$$

where W are the model parameters, $\mathcal{L}_{\text{recon}}$ is the perceptual loss on the image patches, and \mathcal{L}_{seg} is the L1 loss between the predicted and ground truth SDFs: $\mathcal{L}_{\text{seg}} = \|\hat{s}_0 - s_0\|_1$. This formulation provides a robust and well-founded approach to jointly optimizing both the image synthesis and geometric segmentation tasks.

3.3 Semi-Supervised Training Strategy

To effectively leverage the entire OxAAA dataset, which contains 65 cases with both NCCT-CECT pair and lumen mask and 199 cases without lumen mask, we introduce a semi-supervised learning framework. Rather than incorporating complex SSL frameworks, we adopt a direct semi-supervised strategy, leveraging the inherent representation learning strengths of the diffusion model. Our strategy is designed to integrate both data types into the training process seamlessly, addressing the common challenge of label scarcity in clinical applications. The training proceeds in two phases. First, we perform a pre-training phase where the model is warmed up exclusively on the 65 fully-labeled samples for one epoch. This ensures the segmentation head receives a stable initial gradient signal. Following this, we begin the mixed-training phase, where each training batch is constructed by sampling from both the labeled and unlabeled pools at a 1:1 ratio. For samples with ground truth segmentation, the model is optimized using the combined loss mentioned in the previous subsection. For samples lacking a segmentation mask, the segmentation loss is omitted, and the network is updated solely by the reconstruction loss. This allows the shared feature backbone of our diffusion model to learn robust anatomical representations from the entire corpus of 264 cases. The overall semi-supervised training strategy is illustrated in Figure 3 (a).

AortaDiff Workflow During training, the AortaDiff model follows the conditional diffusion model framework: the clean CECT image x_0 is progressively noised to obtain a corrupted version x_t , while the corresponding NCCT scan serves as the conditional input throughout the reverse denoising process. At each timestep t , the model receives the concatenated pair (x_t, NCCT) along with the timestep embedding, and predicts both the noise \hat{e}_t for image reconstruction and the signed distance function (SDF) \hat{s}_0 for lumen segmentation. These two outputs are supervised based on label availability: when both CECT and lumen annotations are available, the model is trained using a multi-task objective. When the lumen mask is unavailable, only the reconstruction loss is applied. During inference, the model takes only the NCCT image as input. Starting from Gaussian noise, it performs iterative denoising conditioned on the NCCT over the full diffusion trajectory. The final outputs are the synthesized CECT image and the corresponding lumen mask. The inference workflow is shown in Figure 3 (b).

4 Experiments

We train and evaluate the proposed multi-tasking diffusion models, AortaDiff, on the Abdominal Aortic Aneurysm dataset released by the Oxford Abdominal Aortic Aneurysm (OxAAA) Study [8, 13]. We assess two variants of our model: **AortaDiff-F**, trained with full supervision on fully-labeled data, and **AortaDiff-P**, trained with incomplete labels using our semi-supervised strategy on the entire dataset.

Performance is assessed on two fronts: synthetic CECT image generation and segmentation of the aortic lumen and thrombus. For each task, we compare our method against state-of-the-art single-task models trained with full supervision. In the segmentation task, we also evaluate the multi-stage baselines that first generate synthetic CECT and then segment the result. Both qualitative and quantitative results demonstrate the effectiveness of our proposed approach.

4.1 OxAAA Dataset

The OxAAA dataset consists of 264 patient cases, each including spatially registered NCCT and CECT scans [13]. Aorta segmentation labels are available for all cases, while only 65 cases additionally include expert-annotated lumen masks. We use 45 of the labeled cases for training and validation, and reserve 20 for testing. In our semi-supervised setting, the remaining 199 cases without lumen annotations are used during training.

4.2 Dataset Preprocessing

All CT scans used in our study are 3D volumes from which we extract 2D slices along the axial plane. To reduce redundancy from high inter-slice similarity, we retain one out of every three axial slices per volume, thereby balancing dataset size and information content. To ensure spatial alignment between NCCT and CECT scans, we retain only slice pairs with an aorta mask dice score above 0.9.

As lumen annotations are available only on the CECT scans, we transfer the corresponding lumen mask to the aligned NCCT slice. This process yields a total of 4,370 paired triplets, each consisting of an NCCT slice, its aligned CECT counterpart, and a corresponding lumen segmentation mask.

From these, we randomly select 2,823 triplets for training and 1,547 for testing. To avoid data leakage, all slices from the same patient are assigned exclusively to either the training or testing split. In addition, we include 7,366 NCCT-CECT slice pairs without lumen annotations, which are used during semi-supervised training.

Hounsfield Units are clipped to the range $[-1000, 1000]$, followed by min-max normalization to $[-1, 1]$ on a per-slice basis before input to the model.

4.3 Experimental Settings

We adopt the AdamW optimizer with a learning rate of 1×10^{-4} and no weight decay [24]. The model is trained with a batch size of 16 and an input image resolution of 256×256 . Training is conducted for a total of 10^6 iterations.

For the DDPM, we use a linear noise schedule with 1,000 diffusion timesteps.

4.4 Evaluation Metrics

For the image generation task, we evaluate the quality of the synthesized CECT slices using Peak Signal-to-Noise Ratio (PSNR), Structural Similarity Index Measure (SSIM) [25], and Learned Perceptual Image Patch Similarity (LPIPS) [21]. Given the anatomical misalignment between the NCCT and CECT, particularly outside the aorta region, we focus our evaluation on the region of interest — the aorta. To reduce the influence of background artifacts and registration errors, we crop each slice to the smallest bounding box that encloses the aorta and compute the metrics within this cropped region.

4.5 Baselines

Synthetic CECT Generation. To evaluate the performance of our method on synthetic CECT generation, we consider two baseline architectures: a U-Net [26] and a conditional diffusion model (CDM) [27]. The noise prediction network used in all diffusion models, including our proposed method, shares the same U-Net backbone for a fair architectural comparison. For the CDM baseline, we evaluate two variants:

CDM-W (Whole Image): The entire NCCT slice is used as the conditioning input to generate the full CECT image.

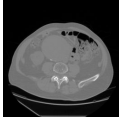
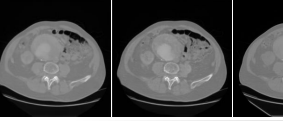
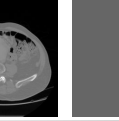
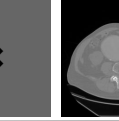
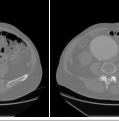
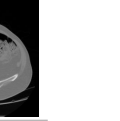
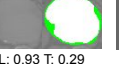
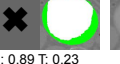
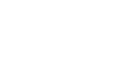
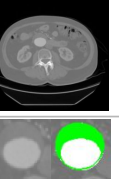
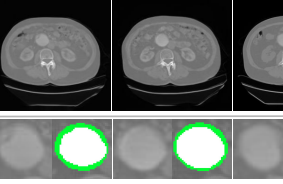
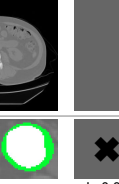
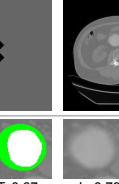
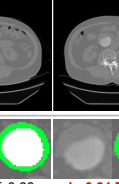
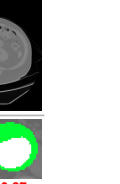
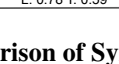
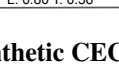
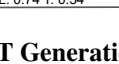
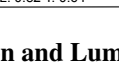
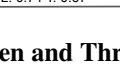
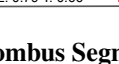
	Input NCCT and GT CECT		Generation Only Methods			Segmentation Only Methods		Multi-Task Methods	
	Real NCCT	Real CECT	UNet	CDM-W	CDM-A	nnUNet	MedSAM	AortaDiff-F	AortaDiff-P
Case 1									
									
Case 2									
									

Figure 4: **Qualitative Comparison of Synthetic CECT Generation and Lumen and Thrombus Segmentation.** This figure illustrates two representative cases comparing generation-only (two-stage pipeline), segmentation-only, and our proposed multi-task methods. For each case, the top row displays the full generated image, while the bottom row provides a zoomed-in view of the aortic region with the corresponding segmentation result. In both cases, our multi-task methods achieve the most accurate segmentation with clearly defined boundaries and precise localization. Note that for generation-only methods, the segmentation is performed by nnU-Net on the generated synthetic CECT. For segmentation-only methods, no synthetic CECT is produced; thus, the corresponding CT images are shown in gray.

CDM-A (Aorta-Restricted): Generation is restricted to the aortic region by conditioning only within the bounding box of the aorta.

This comparison allows us to assess whether focusing generation on the anatomically relevant region yields better results than generating the entire image.

Lumen Segmentation. For the lumen segmentation task, we compare our method with nnU-Net [28], a state-of-the-art self-configuring medical image segmentation framework that achieves strong performance across a wide range of datasets. Additionally, we include MedSAM [29], a pretrained vision foundation model for medical image segmentation. For MedSAM, we use the publicly released pretrained weights without any task-specific fine-tuning.

4.6 Experiment Results

4.6.1 Quantitative Evaluation of CECT Synthesis

Table 1 presents quantitative results for CECT synthesis task, evaluated within the local aortic region. We observe that our proposed aorta-restricted generation strategy (CDM-A) outperforms both CDM-W and U-Net across all metrics. While diffusion models generally yield higher-fidelity outputs than U-Net, CDM-W, which conditions on the entire NCCT slice, underperforms U-Net. This performance gap highlights the diffusion model’s sensitivity to irrelevant regions in the conditioning input, such as those introduced by imperfect alignment between NCCT and CECT scans. These findings underscore the necessity of region-of-interest-focused generation to ensure stable performance in anatomically localized tasks.

Our proposed multi-task diffusion models (AortaDiff-F and AortaDiff-P) achieve the best and second-best performance across all evaluation metrics. This consistent improvement demonstrates that incorporating the segmentation task enhances the model’s ability to capture meaningful anatomical structure, thereby improving image synthesis quality. The results support the hypothesis that joint learning enables the model to leverage semantic guidance from the segmentation objective, leading to more accurate and anatomically coherent CECT generation.

4.6.2 Quantitative Evaluation of Lumen and Thrombus Segmentation

We evaluate lumen segmentation performance directly using each model’s predicted segmentation output. For thrombus segmentation, we first obtain aorta masks at test time using the pretrained nnU-Net described above. We then compute the thrombus mask by subtracting the predicted lumen region from the aorta region. This subtraction-based approach

Method	PSNR (dB) \uparrow	SSIM \uparrow	LPIPS \downarrow
<i>Generation-Only Methods</i>			
UNet	24.40	0.7785	0.0815
CDM-W	23.80	0.7616	0.0859
CDM-A	25.25	0.8137	0.0750
<i>Multi-Task Methods (Ours)</i>			
AortaDiff-F	25.61	0.8385	<u>0.0671</u>
AortaDiff-P	25.48	0.8296	0.0606

Table 1: **Quantitative Comparison on the NCCT-to-CECT Translation Task.** All metrics are computed within the local region surrounding the aorta. The best and second-best values are highlighted in **bold** and underlined, respectively. Our multi-task diffusion models outperform baselines in all metrics.

Method	Lumen Dice Score \uparrow	Thrombus Dice Score \uparrow
<i>Segmentation-Only Methods</i>		
MedSAM	0.7479	0.4356
nnUNet	0.8718	0.4750
<i>Generation-Only Methods (seg. by nnUNet)</i>		
UNet	0.8078	0.4604
CDM-W	0.7748	0.4339
CDM-A	<u>0.8908</u>	0.4914
<i>Multi-Task Methods (Ours)</i>		
AortaDiff-F	0.8887	<u>0.5182</u>
AortaDiff-P	0.8933	0.5326

Table 2: **Quantitative Comparison on the Lumen and Thrombus Segmentation Tasks.** For generation-only methods, segmentation is performed by applying nnU-Net to the generated synthetic CECT images. Our semi-supervised multi-task diffusion models achieve superior performance on both tasks.

aligns with clinical definitions, where the thrombus is the area enclosed by the aortic wall but outside the contrast-filled lumen.

Table 2 presents Dice scores for both lumen and thrombus segmentation. We compare three groups of models: (1) segmentation-only baselines (MedSAM and nnU-Net), (2) generation-only methods, where nnU-Net is applied to synthetic CECT images, and (3) our proposed multi-task diffusion models (AortaDiff-F and AortaDiff-P).

The results reveal several key findings. First, for generation-only method, CDM-A outperforms both CDM-W and U-Net in both tasks, confirming that ROI-constrained generation improves downstream segmentation quality. Second, AortaDiff-P achieves the highest Dice scores across both tasks, 0.8933 for lumen and 0.5326 for thrombus, exceeding even fully supervised segmentation-only methods.

Thrombus segmentation remains more challenging than lumen segmentation, as indicated by lower Dice scores. This is likely due to the thrombus often appearing as thin rings with fewer pixels. Nevertheless, the superior performance of our AortaDiff models suggests that jointly optimizing the generation and segmentation tasks allows the model to learn more accurate anatomical representations of the lumen and surrounding structures.

Importantly, our semi-supervised setup enables the model to benefit from training data without lumen segmentation labels. Even in such cases, the translation task facilitates learning structural cues that improve segmentation performance. This is particularly valuable in real-world clinical settings, where unlabeled imaging data are abundant, but high-quality annotations are expensive and labor-intensive to obtain. By learning jointly from both labeled and unlabeled data, our model demonstrates strong cross-task generalization.

4.6.3 Qualitative Evaluation of CECT Synthesis and Lumen/Thrombus Segmentation

Figure 4 presents two challenging clinical cases to qualitatively compare all baseline and proposed methods across both the CECT synthesis and segmentation tasks.

Table 3: **Lumen Diameter Regression on the Test Set.** Best per column in **bold**.

Method	MAE (mm) ↓	RMSE (mm) ↓	Pearson r ↑
<i>Baseline</i>			
nnU-Net	5.78	9.90	0.91
<i>Ours</i>			
AortaDiff-F	4.70	7.05	0.93
AortaDiff-P	4.19	6.34	0.94

Table 4: **Thrombus Area Prediction Error vs. Ground Truth.** Best per column in **bold**.

Method	Mean \pm SD (%) ↓
<i>Baseline</i>	
nnU-Net	41.45% \pm 29.53%
<i>Ours</i>	
AortaDiff-F	36.89% \pm 19.39%
AortaDiff-P	33.85% \pm 16.52%

In Case 1, the reference CECT reveals a large, circular lumen with a thin but clearly visible mural thrombus encircling the vessel wall, corresponding to a circumferential thrombus morphology. UNet and CDM-W fail to synthesize the enhanced lumen correctly, exhibiting mottled textures and anatomically implausible aortic appearances. While CDM-A recovers a large circular lumen, it lacks contrast enhancement and fails to delineate the aortic boundary. In contrast, AortaDiff-F and AortaDiff-P produce sharper, anatomically realistic lumen enhancement and better preserve the aortic wall. On the segmentation task, AortaDiff models accurately localize the lumen, achieving the highest Dice scores among all methods. Although the thrombus in this case is relatively thin and thus difficult to delineate precisely, both AortaDiff variants outperform all comparison methods in identifying its presence and extent.

In Case 2, the thrombus extends along the posterolateral and lateral walls of the aorta, while the lumen appears as a bright, elliptical structure located in the inferior portion of the aortic cross-section. Only AortaDiff-P correctly synthesizes the shape, contrast, and position of the lumen, along with a clear interface between lumen and thrombus. For segmentation, other methods incorrectly predict the lumen as a large, centrally located circle, leading to under-segmentation of the thrombus. In contrast, AortaDiff models yield accurate segmentation of both the inferolaterally located lumen and the eccentric thrombus.

These results demonstrate that our multi-task diffusion models not only generate anatomically consistent synthetic CECT images but also deliver clinically meaningful segmentation results.

4.7 Clinical Measurements for AAA

Aneurysm morphology is important for predicting AAA progression [13, 30]. We evaluate two clinically relevant metrics, lumen diameter and thrombus area, on a random sample of ten test cases. As shown in Tables 3 and 4, our models produce accurate predictions on both metrics and outperform nnU-Net, indicating strong potential for clinical application.

5 Conclusions

In this work, we introduced AortaDiff, a unified multi-task diffusion framework for generating synthetic CECTs and segmenting the aortic lumen directly from NCCT scans. We demonstrated that having a diffusion model perform these tasks simultaneously enhances performance across both synthesis and segmentation. We also showed that an aorta-focused generation strategy with a background fusion technique can overcome significant data misalignment issues, while a direct, semi-supervised training scheme enables effective learning from annotation-scarce clinical datasets. Experimentally, our multitasking approach significantly outperformed state-of-the-art single-task and multi-stage baselines on both synthesis and segmentation, leading to more accurate AAA clinical measurements. Ultimately, this research represents a meaningful step towards creating a “digital contrast” for CT. By reducing the reliance on iodinated contrast agents, such AI-driven workflows can enhance patient safety, lower procedural costs, and minimize the environmental impact of medical waste, contributing to a more sustainable and climate-neutral healthcare system.

Acknowledgements

We acknowledge the contribution by the OxAAA Study Investigators (in particular Ashok Handa, Pierfrancesco Lapolla and Anirudh Chandrashekhar) and the support by the Thames Valley Vascular Services, Oxfordshire, UK.

References

- [1] Vinicio Napoli, Irene Bargellini, Savino G Sardella, Pasquale Petruzzi, Roberto Cioni, Claudio Vignali, Mauro Ferrari, and Carlo Bartolozzi. Abdominal aortic aneurysm: contrast-enhanced us for missed endoleaks after endoluminal repair. *Radiology*, 233(1):217–225, 2004.
- [2] Gail Ter Haar. Safety and bio-effects of ultrasound contrast agents. *Medical & biological engineering & computing*, 47(8):893–900, 2009.
- [3] Martina C Holder, Daniel A Lewis, and P Shane Winstead. Preventing the harm of a closer look: contrast-induced nephropathy in adults. *Orthopedics*, 35(4):298–303, 2012.
- [4] Margo O Kaller and Jason An. Contrast agent toxicity. 2019.
- [5] Gianmarco Santini, Lorena M Zumbo, Nicola Martini, Gabriele Valvano, Andrea Leo, Andrea Ripoli, Francesco Avogliero, Dante Chiappino, and Daniele Della Latta. Synthetic contrast enhancement in cardiac ct with deep learning. *arXiv preprint arXiv:1807.01779*, 2018.
- [6] Huiqiao Xie, Yang Lei, Tonghe Wang, Pretesh Patel, Walter J Curran, Tian Liu, Xiangyang Tang, and Xiaofeng Yang. Generation of contrast-enhanced ct with residual cycle-consistent generative adversarial network (res-cyclegan). In *Medical Imaging 2021: Physics of Medical Imaging*, volume 11595, pages 1042–1048. SPIE, 2021.
- [7] Jaehee Chun, Jee Suk Chang, Caleb Oh, InKyung Park, Min Seo Choi, Chae-Seon Hong, Hojin Kim, Gowoon Yang, Jin Young Moon, Seung Yeun Chung, et al. Synthetic contrast-enhanced computed tomography generation using a deep convolutional neural network for cardiac substructure delineation in breast cancer radiation therapy: a feasibility study. *Radiation Oncology*, 17(1):83, 2022.
- [8] Anirudh Chandrashekhar, Ashok Handa, Pierfrancesco Lapolla, Natesh Shivakumar, Raman Uberoi, Vicente Grau, and Regent Lee. A deep learning approach to visualize aortic aneurysm morphology without the use of intravenous contrast agents. *Annals of Surgery*, 277(2):e449–e459, 2023.
- [9] Nicolae-Cătălin Ristea, Andreea-Iuliana Miron, Olivian Savencu, Mariana-Iuliana Georgescu, Nicolae Verga, Fahad Shahbaz Khan, and Radu Tudor Ionescu. Cytran: A cycle-consistent transformer with multi-level consistency for non-contrast to contrast ct translation. *Neurocomputing*, 538:126211, 2023.
- [10] Tao Hu, Masahiro Oda, Yuichiro Hayashi, Zhongyang Lu, Kanako Kunishima Kumamaru, Toshiaki Akashi, Shigeki Aoki, and Kensaku Mori. Aorta-aware gan for non-contrast to artery contrasted ct translation and its application to abdominal aortic aneurysm detection. *International Journal of Computer Assisted Radiology and Surgery*, pages 1–9, 2022.
- [11] Qikui Zhu, Yanqing Wang, Shaoming Zhu, and Bo Du. Partial consistent adversarial unified framework for unsupervised non-contrast ct cross-domain adaptation and segmentation. *Pattern Recognition*, 165:111638, 2025.
- [12] Ghazal Azarfar, Seok-Bum Ko, Scott J Adams, and Paul S Babyn. Applications of deep learning to reduce the need for iodinated contrast media for ct imaging: a systematic review. *International journal of computer assisted radiology and surgery*, 18(10):1903–1914, 2023.
- [13] Zachary L Whaley, Ismail Cassimjee, Zdenek Novak, David Rowland, Pierfrancesco Lapolla, Anirudh Chandrashekhar, Benjamin J Pearce, Adam W Beck, Ashok Handa, Regent Lee, Oxford Abdominal Aortic Aneurysm Study, and Oxford Regional Vascular Services. The spatial morphology of intraluminal thrombus influences type II endoleak after endovascular repair of abdominal aortic aneurysms. *Ann Vasc Surg*, 66:77–84, August 2019.
- [14] Zineng Tang, Ziyi Yang, Chenguang Zhu, Michael Zeng, and Mohit Bansal. Any-to-any generation via composable diffusion, 2023.
- [15] Yuqi Yang, Peng-Tao Jiang, Qibin Hou, Hao Zhang, Jinwei Chen, and Bo Li. Multi-task dense predictions via unleashing the power of diffusion. In *The Thirteenth International Conference on Learning Representations*.
- [16] Hanrong Ye and Dan Xu. Diffusionmtl: Learning multi-task denoising diffusion model from partially annotated data, 2024.
- [17] Lanqing Guo, Chong Wang, Wenhan Yang, Siyu Huang, Yufei Wang, Hanspeter Pfister, and Bihan Wen. Shadowdiffusion: When degradation prior meets diffusion model for shadow removal, 2022.

- [18] Ruchika Chavhan, Abhinav Mehrotra, Malcolm Chadwick, Alberto Gil Ramos, Luca Morreale, Mehdi Noroozi, and Sourav Bhattacharya. Upcycling text-to-image diffusion models for multi-task capabilities, 2025.
- [19] Hantao Zhang, Yuhe Liu, Jiancheng Yang, Weidong Guo, Xinyuan Wang, and Pascal Fua. Diffatlas: Genai-fying atlas segmentation via image-mask diffusion, 2025.
- [20] Hantao Zhang, Yuhe Liu, Jiancheng Yang, Shouhong Wan, Xinyuan Wang, Wei Peng, and Pascal Fua. Lefusion: Controllable pathology synthesis via lesion-focused diffusion models, 2024.
- [21] Richard Zhang, Phillip Isola, Alexei A. Efros, Eli Shechtman, and Oliver Wang. The unreasonable effectiveness of deep features as a perceptual metric, 2018.
- [22] Andreas Lugmayr, Martin Danelljan, Andres Romero, Fisher Yu, Radu Timofte, and Luc Van Gool. Repaint: Inpainting using denoising diffusion probabilistic models, 2022.
- [23] Alex Kendall, Yarin Gal, and Roberto Cipolla. Multi-task learning using uncertainty to weigh losses for scene geometry and semantics, 2018.
- [24] Ilya Loshchilov and Frank Hutter. Decoupled weight decay regularization, 2019.
- [25] Zhou Wang, A.C. Bovik, H.R. Sheikh, and E.P. Simoncelli. Image quality assessment: from error visibility to structural similarity. *IEEE Transactions on Image Processing*, 13(4):600–612, 2004.
- [26] Olaf Ronneberger, Philipp Fischer, and Thomas Brox. U-net: Convolutional networks for biomedical image segmentation, 2015.
- [27] Prafulla Dhariwal and Alex Nichol. Diffusion models beat gans on image synthesis, 2021.
- [28] Fabian Isensee, Paul F Jaeger, Simon A A Kohl, Jens Petersen, and Klaus H Maier-Hein. nnU-Net: a self-configuring method for deep learning-based biomedical image segmentation. *Nature Methods*, 18(2):203–211, February 2021.
- [29] Jun Ma, Yuting He, Feifei Li, Lin Han, Chenyu You, and Bo Wang. Segment anything in medical images. *Nature Communications*, 15(1):654, January 2024.
- [30] Anders Wanhanen, Fabio Verzini, Isabelle Van Herzele, Eric Allaire, Matthew Bown, Tina Cohnert, Florian Dick, Joost van Herwaarden, Christos Karkos, Mark Koelemay, Tilo Kölbel, Ian Loftus, Kevin Mani, Germano Melissano, Janet Powell, Zoltán Szeberin, Esvs Guidelines Committee, Gert J de Borst, Nabil Chakfe, Sebastian Debus, Rob Hinchliffe, Stavros Kakkos, Igor Koncar, Philippe Kolh, Jes S Lindholt, Melina de Vega, Frank Vermassen, Document Reviewers, Martin Björck, Stephen Cheng, Ronald Dalman, Lazar Davidovic, Konstantinos Donas, Jonothan Earnshaw, Hans-Henning Eckstein, Jonathan Golledge, Stephan Haulon, Tara Mastracci, Ross Naylor, Jean-Baptiste Ricco, and Hence Verhagen. Editor’s choice - european society for vascular surgery (ESVS) 2019 clinical practice guidelines on the management of abdominal aorto-iliac artery aneurysms. *Eur J Vasc Endovasc Surg*, 57(1):8–93, December 2018.